Inverted-S Antenna with Wideband Circular Polarization and Wide Axial Ratio Beamwidth

Long Zhang, Steven Gao, Member, IEEE, Qi Luo, Member, IEEE, Paul Young, Senior Member, IEEE, Wenting Li, Qingxia Li, Member, IEEE

Abstract—A novel broadband circularly polarized (CP) antenna with wide axial ratio (AR) beamwidth is proposed. It is composed of two curved arms shaped like an inverted "S". The mechanisms of wideband CP operation and wide AR beamwidth are explained. To validate the concept, a prototype at C-band is manufactured and measured. Experimental results confirm that the antenna achieves an impedance bandwidth of 63% and a CP bandwidth of 42%. Furthermore, maximum AR beamwidth of 140° is achieved and wide AR beamwidth can be maintained in a frequency bandwidth of 35% in nearly all elevation planes. In addition, the antenna has the advantage of being easily extended to arrays. A 4-element array using the proposed antenna is investigated through both simulations and experiments, and achieves 60% CP bandwidth and wide AR beamwidth. The proposed inverted-S antenna can realize wide CP bandwidth and wide AR beamwidth, and is easy to form wideband CP arrays.

Index Terms—Circular polarization, broadband antennas, wide axial ratio beamwidth, wideband array.

I. Introduction

CIRCULARLY POLARIZED (CP) antennas are widely deployed in various wireless systems due to their advantages of the mitigation of multipath fading, the reduction of 'Faraday rotation' and the immunity of polarization mismatching between transmitting and receiving antennas [1]. Extensive research work on improving the AR bandwidth (AR<3dB) of CP antennas has been reported, as the traditional microstrip patches with perturbations exhibit less than 5% bandwidth [2]. Dual-feed technique and 90° hybrid were used to increase the CP bandwidth [3]. Other antennas, such as stacked patches [4], slot antenna [5] and magneto-electric dipole [6] are also good candidates for wideband CP operation.

Besides improving the AR bandwidth, widening the AR beamwidth of CP antennas was received increasing interest due to their applications in global navigation satellite systems (GNSS) [7] and wide-angle CP beam-scanning array [8]. Several researches on this topic were reported including a square-ring slotted patch antenna [9], an asymmetric microstrip antenna with integrated circular-patches [10] and an elliptical vertical patch antenna backed by an elliptical air cavity [11]. Although these CP antennas can achieve more than 120° AR beamwidth, their AR bandwidths are smaller than 5%. For some applications, such as covering all GNSS bands, these antennas may not applicable.

To meet the system requirement of large bandwidth, normally the antenna needs to be designed either as multiband or wideband. The multi-band CP antennas with wide AR beamwidth in each working band can be found in [12-14]. In [12], a multi-branch crossed dipole was presented with more than 110° AR beamwidth. Stacked cone-patches were used to achieve dual-band operation and over 110° AR beamwidth [13]. A novel dual-frequency dual CP patch antenna with orthogonal and offset-centered slots was reported in [14], which realized RHCP (right-hand circular polarization) and LHCP (left-hand circular polarization) at two different bands with more than 160° AR beamwidth. However, for high date rate satellite communications, it is always desirable to have a wideband antenna with wide AR beamwidth especially for the receivers.

Despite the importance of wideband CP antennas with wide AR beamwidth, there are few reported researches. Two pairs of parallel dipoles were orthogonally placed in a square contour and were excited in phase quadrature to acquire wide AR beamwidth when the space between the parallel dipoles was appropriately chosen [15]. The AR bandwidth of this antenna is from 1.52GHz to 1.65GHz (8.2%) and 126° AR beamwidth is achieved at 1.6GHz. However, the AR beamwidth may degrade when frequency shifts away from 1.6GHz. A stacked patch antenna with 10.2% CP bandwidth and 140° AR beamwidth was presented in [16]. Likewise, the AR beamwidth is measured at only 2.4GHz and the AR beamwidths at other frequency points within the working band are not provided. In [17], a wideband magneto-electric dipole which has 33% AR bandwidth and 85° AR beamwidth within the AR passband in the two main planes was reported. Stable wide angular CP radiation could also be observed in [18], where a crossed dipole was loaded with a magneto-electric dipole to realize good CP performance. In [18], 27.7% AR bandwidth was achieved and over 165° AR beamwidth could be realized from 1.45GHz to 1.7GHz (15.8%) in the two main planes. Although the antenna presented in [17, 18] can achieve wideband CP radiation with wide angular CP coverage in the two main planes, it is not clear whether wide AR beamwidths can be maintained in other

L. Zhang, S. Gao, Q. Luo, P. R. Young and W. Li are with the School of Engineering and Digital Arts, University of Kent, Canterbury CT2 7NT, UK. (emails: lz76@kent.ac.uk; s.gao@kent.ac.uk).

Q. Li is with the School of Electronic Information and Communications, Huazhong University of Science and Technology, Wuhan 430074, China.

elevation planes. Moreover, these antennas have complicated structures, which make them difficult to be implemented in wideband CP arrays.

In this paper, a novel inverted S-shaped CP antenna with a simple configuration is presented, which achieves wide CP bandwidth and wide AR beamwidth simultaneously. Stable wide angular CP radiation characteristics are maintained in a wide frequency range in the XOZ plane. In other elevation planes, the AR beamwidths are wider than the half power beamwidths (HPBWs). Compared with other reported antennas, the proposed antenna achieves a wider CP bandwidth and a more stable AR beamwidth within the operational bandwidth. Moreover, it can be easily extended to a wideband CP array with wide AR beamwidth, which is also discussed in this paper.

This paper is organized as follows: Section II introduces the antenna configuration and operational principles of wide angular CP radiation; Section III presents the simulation results and measurement results of the proposed antenna as well as the comparison with other reported antennas; Section IV presents a linear array consisting of the proposed antenna element and the results of this array; the conclusion is given in Section V.

II. Antenna Configuration and Operational Principles

A. Antenna Configuration

The configuration and geometry dimensions of the proposed antenna are shown in Fig. 1. As shown, the antenna consists of two curved arms and is printed on the bottom layer of a 0.508mm thick Rogers RO4003C substrate with a size of $W_1 \times L_1$. To feed the antenna, an integrated balun which transforms the unbalanced microstrip feed to balanced slot line feed is utilized. The balun is printed on both layers of a 0.813mm thick Rogers RO4003C substrate which has a size of $W_1 \times H_7$. An $L_2 \times L_2$ sized ground plane is placed below the antenna with a distance of H_1, which is mainly used to achieve directional radiation.

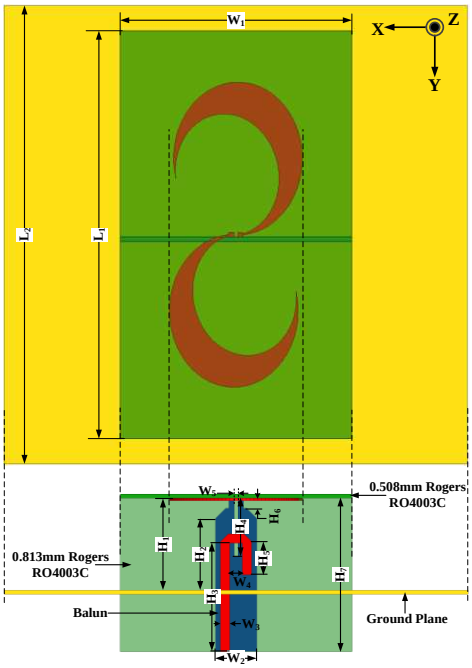

Fig. 1. The geometry of the proposed antenna.

The curved arm can be obtained through cutting a bigger ellipse by a smaller rotated ellipse, as shown in Fig. 2. This method is inspired by [19], where two concentric semi-circles are used to form a vortex slot. As can be seen from Fig. 2, the bigger ellipse has a major axis radius R_1 and minor axis radius R_2 while the smaller ellipse's major and minor axis radius is R_3 and R_4, respectively. To get the desired arm, the smaller ellipse is counterclockwise rotated along point O with an angle of α and then it is subtracted from the bigger ellipse.

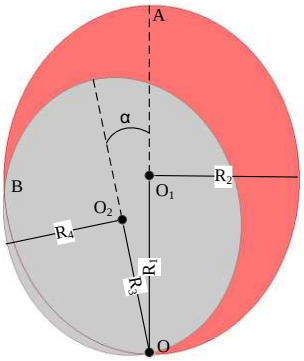

Fig. 2. Detailed geometry of the curved arm.

TABLE I gives the detailed antenna parameters. Besides, the rotation angle α is 10°. The lengths of the outer curve and inner curve are around 65mm and 52mm equaling to about $1.8\lambda_g$ and $1.4\lambda_g$ at the center frequency 5GHz, which provide enough travelling paths for a travelling wave current flowing along the curved arm. The distance between the antenna and the ground plane (H_1) is chosen to be 18mm in order to achieve maximum AR bandwidth. Meanwhile, the antenna gain can also be maintained at a reasonable value at this height. The ground plane size ($L_2 \times L_2$) is determined by taking into consideration of the performance of AR and radiation patterns. Generally, the AR bandwidth degrades but the performance of radiation patterns get enhanced with larger L_2. The size of the ground

plane is chosen to be 90mm × 90mm to achieve wide AR bandwidth and good radiation patterns.

TABLE I
ANTENNA PARAMETERS (MM)

L_1	L_2	W_1	W_2	W_3	W_4	W_5	H_1	H_2
80	90	45	8	1.77	2.46	0.8	18	14
H_3	H_4	H_5	H_6	H_7	R_1	R_2	R_3	R_4
21.5	11.5	6.23	2	30	15	12.5	12	10

B. Operational Principles of Circularly Polarized Radiation

To explain the operational principles of CP radiation, the surface current distribution on the curved arms at different time slot is shown in Fig. 3. As shown, the null area of the surface current is propagating along the curved arms, which is similar to the phenomenon observed in [20]. It is reported in [20] that a travelling wave current is realized along the equiangular strip and aperture edge. Different to [20], in this design the travelling wave current is excited along the curved arms even without any ground plane or cavity, which simplifies the fabrication and makes the presented antenna a better candidate for the array application. Furthermore, the proposed antenna exhibits wide AR beamwidth characteristic which is not observed in [20].

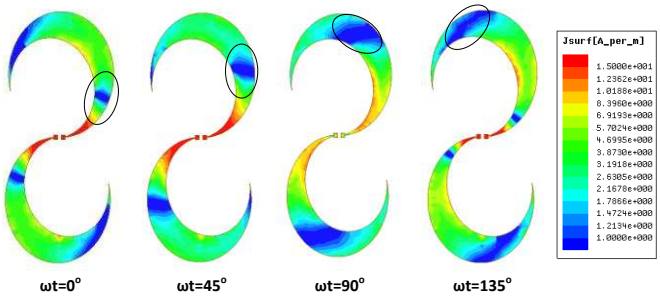

Fig. 3. The surface current on curved arms at different time slots.

C. Mechanism of Wide Angular CP Radiation

Considering that the antenna consists of two curved arms fed by signals out of phase, the far-field radiation of the proposed antenna can be synthesized using a 2-element array. To validate this assumption, a 2-element array was simulated and each curved arm is fed by a lumped port like a horizontal monopole, with 180 ° phase differences between the two ports.

For a fair comparison of the radiated electric field, the distance between the ground plane and the 2-element array is kept 18mm, the same as the height of the proposed antenna. The proposed antenna is fed by a lumped port to eliminate the influences of the balun. Fig. 4 shows the comparison of radiation patterns in RHCP and LHCP components between the proposed antenna and the 2-element array at 4.7GHz in the XOZ plane. As shown, the far-field radiation between the proposed antenna and the 2-element array is nearly the same. The agreement of the radiation patterns can also be observed at other frequencies and different elevation planes. Therefore, it is reasonable to deem the proposed antenna as a 2-element array as shown in Fig. 5.

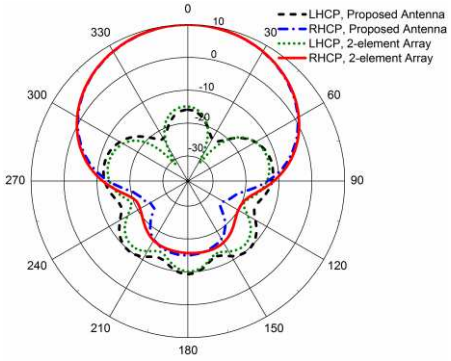

Fig. 4. The radiation patterns of the proposed antenna and the 2-element array in XOZ plane

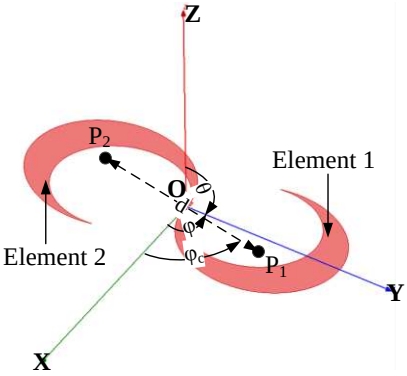

Fig. 5. The geometrical arrangement of 2-element array.

The radiated fields of the proposed antenna can then be obtained by vector summing of the fields radiated by each element (curved arm). As shown in Fig. 5, P_1 and P_2 denote the phase center of each element respectively. Becasue the element 2 is acquired through rotating element 1 by 180° at the origin point O, the points P_1, P_2 and O are in a line. Denoting the distance between P_1 and P_2 by d and the angle between the line P_1OP_2 and axis X by φ_c, the spatial phase delay of the two elements in XOZ plane can then be represented by:

$$\delta = k_0 d \cos\varphi_c \sin\theta \quad (1)$$

where k_0 is the wavenumber in free space. For an elliptically polarized antenna, the radiated electric field of element 1 can be written by [21]:

$$\overrightarrow{E_1}(\theta,\varphi) = a(\theta,\varphi)\overrightarrow{e_\theta} + b(\theta,\varphi)\overrightarrow{e_\varphi}e^{j\frac{\pi}{2}} \quad (2)$$

Here, $a(\theta,\varphi)$ and $b(\theta,\varphi)$ are the amplitude of the two orthogonal unit vectors $\overrightarrow{e_\theta}$ and $\overrightarrow{e_\varphi}$, which are functions of θ and φ. For a qualitative analysis, the total field in XOZ plane is deduced while the fields in other planes can also be derived by using different spatial phase delay between the two elements.

As element 2 is axisymmetric to element 1, the radiated field of element 2 in XOZ plane can be written as follows:

$$\overrightarrow{E_2}(\theta,0) = -\overrightarrow{E_1}(\theta,\pi) = -\overrightarrow{E_1}(-\theta,0) \quad (3)$$

Here, the negative sign stems from the physical rotation angle π which results in a reverse direction of the electric field. The total electric field in XOZ plane is given by:

$$\overrightarrow{E_t}(\theta,0) = \overrightarrow{E_1}(\theta,0) + \overrightarrow{E_2}(\theta,0)e^{j\pi}e^{j\delta} \quad (4)$$

The $e^{j\pi}$ component in (4) comes from the feeding phase difference π. Substituting (2)-(3) into (4) and (4) can be rewritten as

$$\overrightarrow{E_t}(\theta,0) = \overrightarrow{E_1}(\theta,0) + \overrightarrow{E_1}(-\theta,0)e^{j\delta} = \left[a(\theta,0) + a(-\theta,0)e^{j\delta}\right]\overrightarrow{e_\theta} + \left[b(\theta,0) + b(-\theta,0)e^{j\delta}\right]\overrightarrow{e_\varphi}e^{j\frac{\pi}{2}} \quad (5)$$

Equation (5) indicates that the total field $\overrightarrow{E_t}$ in the XOZ plane equals to the summation of field $\overrightarrow{E_1}(\theta,0)$ and $\overrightarrow{E_1}(-\theta,0)e^{j\delta}$. The physical insight of equation (5) is that the total field $\overrightarrow{E_t}$ originates from two elliptically polarized fields while the phase difference between them is δ. Due to the asymmetric radiation pattern to Z axis of each element, $\overrightarrow{E_1}(-\theta,0)$ does not equal to $\overrightarrow{E_1}(\theta,0)$ for a given elevation angle θ (except for $\theta = 0$). Denoting the axial ratio of $\overrightarrow{E_1}(\theta,0)$ by $AR_1(\theta)$ and the axial ratio of $\overrightarrow{E_1}(-\theta,0)$ by $AR_2(\theta)$, then

$$AR_2(\theta) = AR_1(-\theta) = a(-\theta,0)/b(-\theta,0) \quad (6)$$

Also, $AR_2(\theta) \neq AR_1(\theta)$ except for $\theta = 0$. According to (5), for a given θ, the AR of the total field $\overrightarrow{E_t}$ is determined by AR_1 AR_2 and δ. Since $AR_2(\theta) \neq AR_1(\theta)$, it gives the possibility to realize a total field with a better AR_t ($AR_t < AR_1$ *or* AR_2).

To give a more visualized explanation, the phase differences of the RHCP and LHCP electric field component between the two elements in the XOZ plane is given by Fig. 6. For an easier comparison, element 2 is fed with an 180° phase difference to element 1. The far-field RHCP component phase difference is calculated by $Phase_{RHCP,elment\ 1} - Phase_{RHCP,elment\ 2}$ while the phase difference of LHCP component is calculated by $Phase_{LHCP,elment\ 1} - Phase_{LHCP,elment\ 2}$.

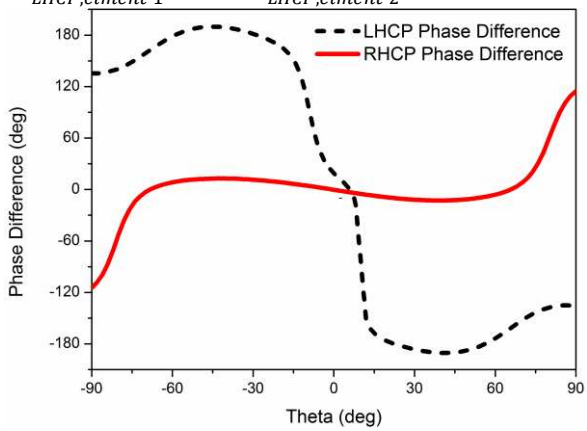

Fig. 6. Phase differences of RHCP and LHCP component between the two elements at 4.7GHz in the XOZ plane.

As shown in Fig. 6, the phase difference of the RHCP component (co-pol component) is around 0° from -70° to 70° angular range. This means that the RHCP components of the two elements are nearly in phase and can be superposed in a wide angular range. Meanwhile, the phase difference of the LHCP component (cross-pol component) is around -180° from 15° to 70° angular range and around 180° from -15° to -70° angular range. The LHCP components of the two elements are therefore canceled by each other in the angular range of 15° to 70° and -15° to -70°. As the RHCP component of the 2-element array gets enhanced and the LHCP component gets decreased in a wide angular range, the AR improves in a wide angular range and wide angular CP radiation can be achieved.

From equation (5), the fields of two elements will be superposed in phase at broadside direction ($\theta = 0$). However, the phased difference of LHCP component is slightly higher than 0°. This phase error is believed to be caused by the mutual coupling between the two elements.

Fig. 7 shows the simulated AR and HPBW of the proposed antenna (without balun) in the upper hemisphere area at 4.7GHz. The dark area denotes regions where the AR is smaller than 3dB and the HPBW is bounded by the two red curves. Fig. 7 clearly demonstrates that the AR beamwidths in each elevation planes are larger than the HPBWs. The decrease of the AR beamwidth is along with the decrease of HPBW, leading to a wide AR beamwidth covering HPBW in the whole upper hemisphere.

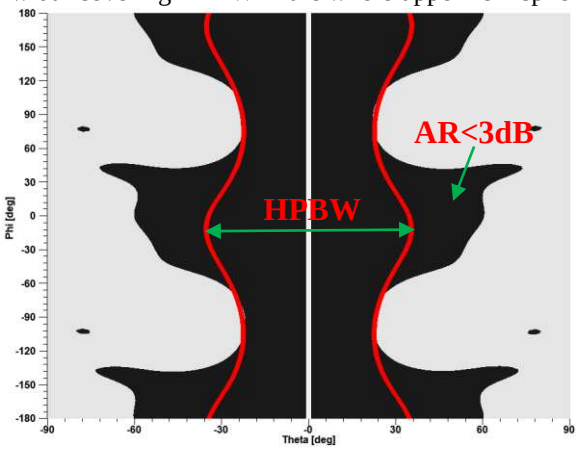

Fig. 7. The Axial Ratio and HPBW of the proposed antenna at 4.7GHz.

III. Results and Discussions

A. The Antenna Prototype and VSWR

The prototype of the proposed antenna is shown in Fig. 8. As shown, a coaxial connector is connected to the end of the balun to feed the antenna. Four plastic pillars are used to support an 18mm air gap between the antenna and the ground plane.

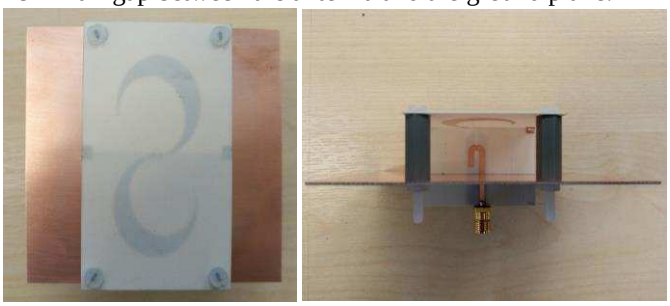

(a) (b)

Fig. 8. The prototype of the proposed antenna: (a) top view, (b) side view.

The simulated and measured VSWR of the proposed antenna is given by Fig. 9. As can be seen, the measured impedance bandwidth (VSWR<2) is from 3.4GHz to 6.5GHz (63%). Compared with the simulated VSWR, the measured result is slightly shifted to lower frequency, which is caused by fabrication and measurement errors.

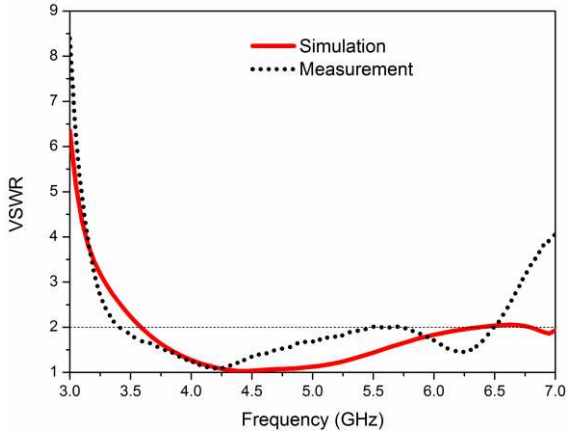

Fig. 9. The simulated and measured VSWR of the proposed antenna.

B. Axial Ratio Bandwidth

The AR bandwidth of the proposed antenna is shown in Fig. 10.

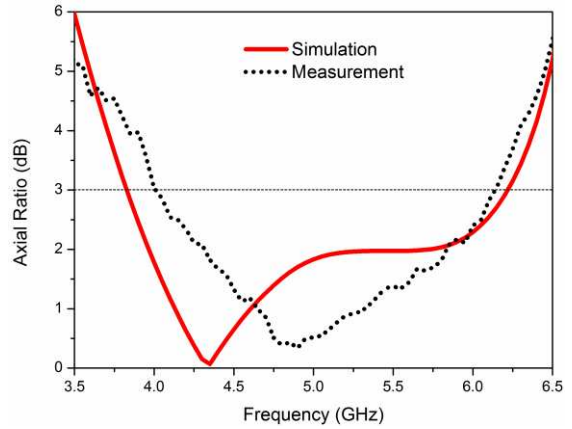

Fig. 10. The simulated and measured AR bandwidth of the proposed antenna.

The measured AR bandwidth (AR<3dB) is from 4GHz to 6.15GHz, results in a fractional bandwidth of 42%. Different to the simulated AR, the frequency of measured minimum AR point is shifted to a higher frequency which is around 5GHz.

C. Axial Ratio Beamwidth

As aforementioned, the proposed antenna exhibits stable wide AR beamwidth apart from its wide AR bandwidth. The stable wide AR beamwidth of the proposed antenna not only rests on its wide AR beamwidth in the symmetric plane (XOZ plane) but also lies in its AR beamwidths in other cutting planes, which are wider than HPBWs.

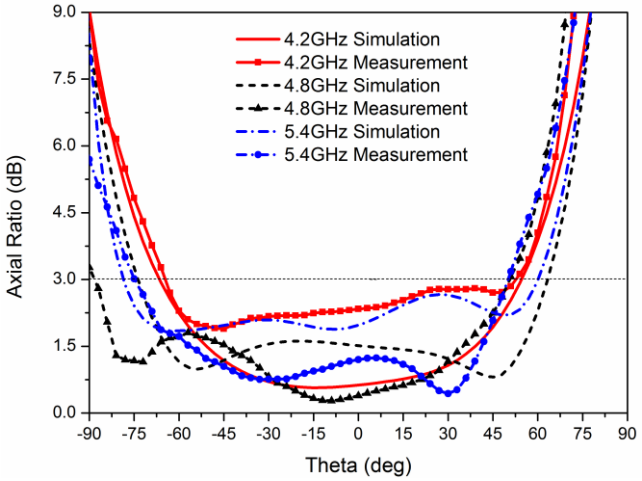

Fig. 11. The simulated and measured AR beamwidth in the XOZ plane at different frequencies.

Fig. 11 shows the simulated and measured AR beamwidth in the XOZ plane at different frequency points. As shown, the measured AR beamwidths in the XOZ plane are 117°, 138° and 123° at 4.2GHz, 4.8GHz and 5.4GHz, respectively. In line with the measured AR bandwidth shown in Fig. 10, the measured AR in other elevation angles is also smaller than the simulated AR in higher frequencies, which also verifies the shifting of minimum AR point to a higher frequency. The difference between the measurement and simulation results may come from the fabrication and measurement errors. It is also observed that the AR beamwidth is asymmetric to $\theta = 0$, which is different to the symmetric AR beamwidth observed in Fig. 7. This asymmetry is caused by the integrated balun which has an asymmetric microstrip line to $\theta = 0$ direction. Although the radiation of this microstrip line is small, it still introduces different influences to the CP radiation in different elevation angle θ [22].

To give an understanding of the AR beamwidths in other cutting planes and the comparison between the AR beamwidths and HPBWs, the value of measured AR beamwidths and measured HPBWs in planes $\varphi = 0^o, 30^o, 60^o, 90^o$ are given by Fig. 12. As can be seen, in elevation planes $\varphi = 0^o, 30^o, 60^o$, the AR beamwidths are larger than the HPBWs from 4GHz to 6GHz. However, in the $\varphi = 90^o$plane, the AR beamwidth is slightly smaller than the HPBW at some frequency points. As the value of AR is determined by the RHCP and LHCP component, slightly increase of cross-pol (LHCP) component makes the AR larger than 3dB and results in a narrower AR beamwidth. In spite of this, the measured results still indicate that the proposed antenna can achieve a wide angular CP radiation in the upper-hemisphere. It is also noticed that the HPBW increases as the frequency goes up in the $\varphi = 0^o$ plane but decreases as the frequency rises in $\varphi = 30^o, 60^o, 90^o$ planes. According to [23], the antenna gain is in reverse proportional to the product of HPBWs in two perpendicular planes. Although the HPBW's variation of the proposed antenna is different in each plane, the product of the HPBWs in each two perpendicular planes always increases as the frequency goes up, indicating a decrease of antenna gain as the

frequency rises, which is verified by Fig. 13.

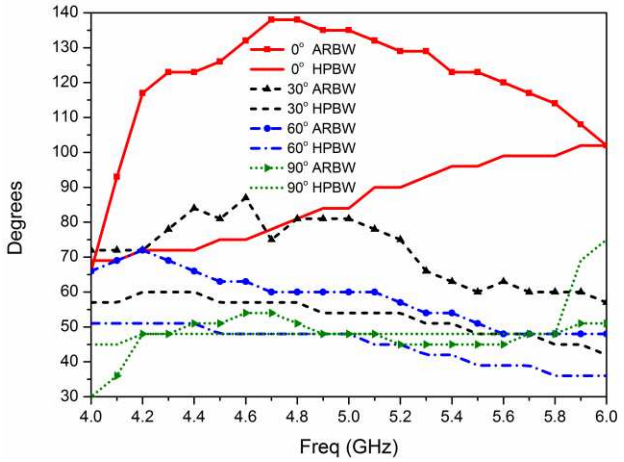

Fig. 12. The measured AR beamwidths and HPBWs in different cutting planes.

D. Radiation Pattern and Antenna Gain

The simulated and measured antenna gain is shown in Fig. 13. As shown, the measured antenna gain is around 9-10dBic from 4 to 5.4GHz. Fig. 13 also shows the simulated efficiency which is larger than 90% across the whole operation bandwidth. It is indicated by the simulation that the insertion loss of the balun increases as the frequency increases, around 0.2dB at 4GHz and 0.8dB at 6GHz. It is worth pointing out that the insertion loss includes dielectric loss, conductor loss and radiation loss. From the simulation, it is found that the radiation loss of the balun accounts for a considerable proportion, which results in a high simulation efficiency shown in Fig. 13.

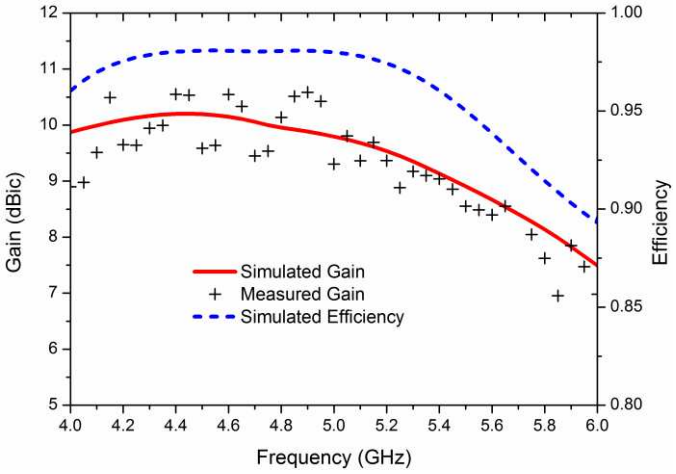

Fig. 13. Antenna gain and simulated efficiency.

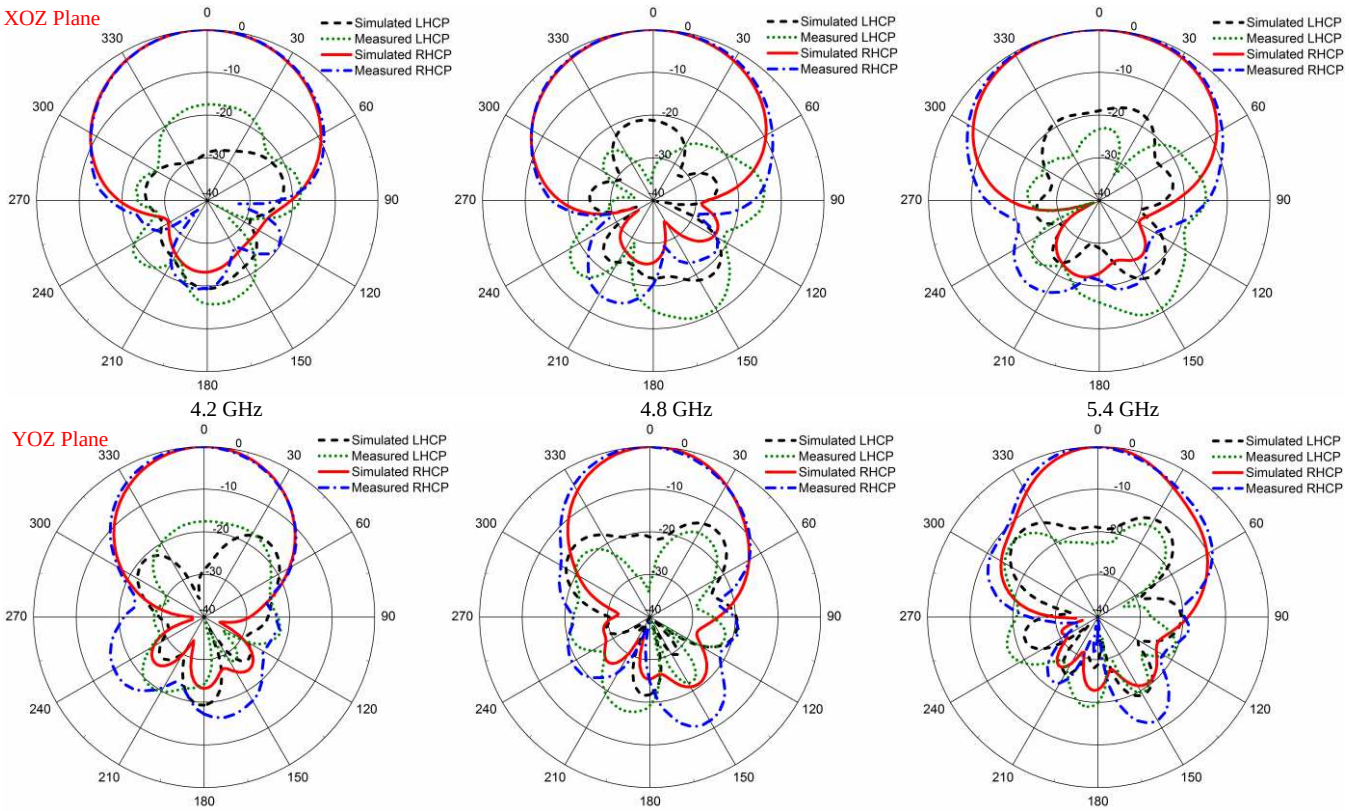

Fig. 14. The measured and simulated radiation patterns of the proposed antenna: top row, XOZ Plane; bottom row, YOZ Plane

The radiation patterns of the proposed antenna at different frequency points are shown in Fig. 14. As can be seen from the figure, good agreements are observed between the simulation and measurement results of all co-pol components (RHCP) in the upper hemisphere region. The differences in the back lobe may cause by the scattering of the cable and antenna holder. To measure the back lobe of the proposed antenna, an antenna holder is fabricated and placed above the positioner, which brings an extension of test cable and antenna holder behind the proposed antenna.

E. Comparison with Other Antennas

To demonstrate the advantages of the proposed antenna, table

TABLE II
COMPARISON WITH OTHER WIDEBAND WIDE AR BEAMWIDTH ANTENNAS

	Antenna Size (mm) and electric length at center freq.	Antenna Size with Ground Plane or Cavity (mm)	Impedance Bandwidth (GHz)	3dB AR Bandwidth (GHz)	Maximum AR beamwidth and corresponding HPBW (°)	AR beamwidth vs Frequency in Main Planes	AR beamwidth in other Elevation Planes	Extension to Antenna Array
[15]	100×100×0.8, 0.53λ×0.53λ×0.004λ	Bidirectional, no ground plane	1.35-1.85, 31%	1.52-1.65, 8.2%	AR beamwidth:126° HPBW: –	—	—	—
[16]	43.7×44.8×11.5, 0.38λ×0.39λ×0.1λ	Not shown	1.85-3.38, 58.5%	2.23-2.47, 10.2%	AR beamwidth:175° HPBW:150°	—	—	—
[17]	150×150×38, 1λ×1λ×0.25λ	150×150×38, 1λ×1λ×0.25λ	1.6-2.42, 40.8%	1.63-2.27, 32.8%	AR beamwidth:85° HPBW:-	AR beamwidth=85° from 1.8 to 2.1GHz (15.4%)	—	—
[18]	76×76×0.5, 0.46λ×0.46λ×0.003λ	120×120×30, 0.73λ×0.73λ×0.18λ	1.27-2.36, 59.8%	1.39-1.82, 26.8%	AR beamwidth:175° HPBW: -	AR beamwidth>165° from 1.45 to 1.7GHz (15.8%)	—	—
Simulated Spiral	58.4×44.8×0.5, 1.11λ×0.85λ×0.01λ	90×90×18, 1.71λ×1.71λ×0.34λ	—	5.15-6.24, 19.1%	AR beamwidth:64.2° HPBW:117°	—	AR beamwidth< HPBW	—
This Work	59.9×25.8×0.5, 0.99λ×0.42λ×0.008λ	90×90×18, 1.48λ×1.48λ×0.3λ	3.4-6.5, 62.6%	4-6.15, 42%	AR beamwidth:142° HPBW:82°	AR beamwidth>100° from 4.2 to 6GHz (35.3%)	AR beamwidth> HPBW	Yes

II compares the proposed antenna with other reported wideband wide AR beamwidth antennas. A 3/4 turn Archimedean spiral was also simulated and compared with the proposed antenna. In order to provide a fair comparison, the spiral antenna was designed by using the same substrate that used for the proposed antenna and the size of the spiral is adjusted to be similar physical size as the presented antenna.

TABLE II gives the comparison between the proposed antenna and other antennas in terms of antenna size, impedance bandwidth, AR bandwidth, and AR beamwidth. From TABLE II, it is shown that the proposed antenna has wider CP bandwidth and more stable AR beamwidth within the operational bandwidth. Moreover, the AR beamwidths of the proposed antenna are larger than the HPBWs in other elevation planes, which were not investigated by other researchers. The antenna is also easy to be extended to an antenna array which is shown in the following section.

IV. Antenna Array and Results

A. Array Configuration

Compared with other reported wideband wide AR beamwidth CP antennas, another advantage of the proposed antenna is that it can be easily extended to an antenna array.

To prove this concept, a four-element linear array is designed and prototyped. Fig. 15 shows the presented antenna array, which consists of 4 inverted S-shaped elements. The element space is 26.5mm which is about $0.35\lambda_0$, $0.44\ \lambda_0$ and $0.53\lambda_0$ for 4GHz, 5GHz and 6GHz, respectively. The small element space was chosen in this design helps enhance the bandwidth of the antenna array, which is also observed in sub-wavelength array [24] and can be explained by the cancelling of the imaginary part of mutual impedances [25]. The presented array is printed on a 0.508mm thick Rogers RO4003C substrate with a size of 65mm × 120mm while a 1:4 power divider is printed on a 0.813mm thick Rogers RO4003C substrate with a size of 60mm × 120mm. Below the antenna board, there is a ground plane with the size of 90mm × 165mm. The distance between the antenna and the ground plane is kept 18mm, which is the same as the antenna element.

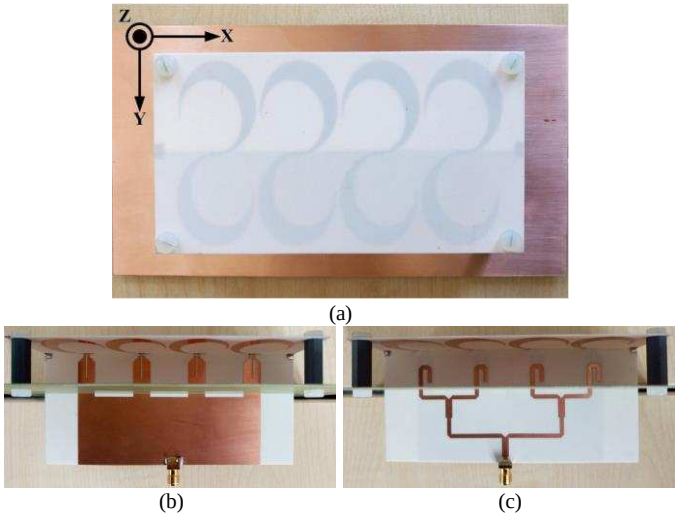

(a) (b) (c)

Fig. 15. The prototype of the proposed array: (a) top view, (b) left side view, (c) right side view.

It is worth pointing out that the ground plane of each balun is also kept the same size as in the antenna element. By doing this, the influence of the balun to the performance of the array can be minimized. This is because reducing the size of the ground plane of the balun effectively decrease the surface current flowing area, which makes the radiation of the balun relatively far away from the radiation region of the antenna [22].

B. VSWR and Axial Ratio Bandwidth

The comparison between the simulated and measured VSWR of the proposed array is shown in Fig. 16. As shown in the figure, the measurement result is in good agreement with the simulation result. The measured impedance bandwidth is from 3.57GHz to 6.3GHz (55.3%).

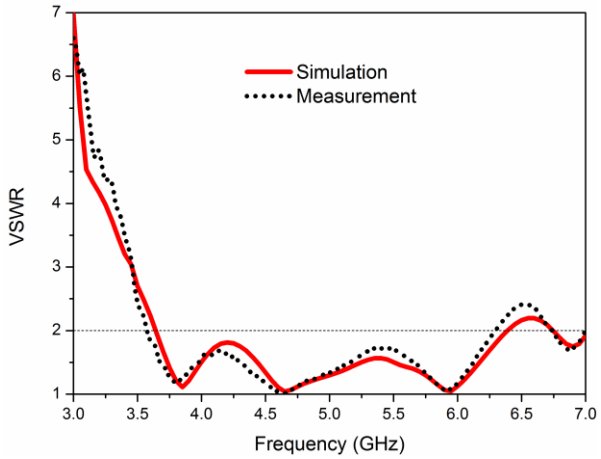

Fig. 16. The simulated and measured VSWR of the proposed array.

The simulated and measured AR of the presented array is given by Fig. 17. The measured CP bandwidth (AR<3dB) of the presented array is from 3.5GHz to 6.5GHz (60%).

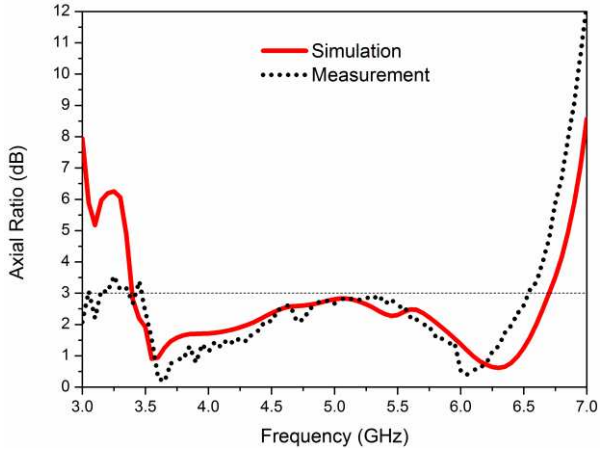

Fig. 17. The simulated and measured AR of the proposed array.

C. Axial Ratio Beamwidth of the Array

To evaluate the AR beamwidth characteristics of the array, Fig. 18 shows the measured AR beamwidths and HPBWs in planes $\varphi = 0^o, 30^o, 60^o, 90^o$. As shown, the AR beamwidths are larger than the HPBWs from 4GHz to 6GHz in elevation

planes $\varphi = 0^o, 30^o, 60^o$. However, the AR beamwidth is smaller than the HPBW in plane $\varphi = 90^o$, which may due to the narrow AR beamwidth of the antenna element in this plane and the effect of mutual coupling between each element.

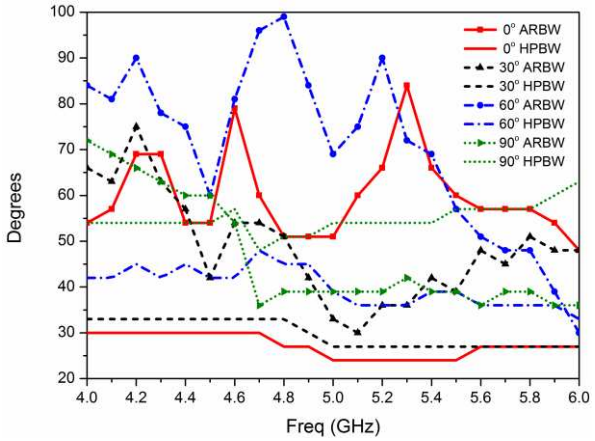

Fig. 18. The measured AR beamwidths and HPBWs of the array.

D. Radiation Pattern and Gain

To evaluate the radiation performance of the presented array, radiation patterns of the proposed array at 4GHz and 6GHz are given by Fig. 19. As shown, the measurement results agree well with the simulation results. Better agreements are obtained due to the fact that the array antenna has a larger ground plane which provides better shielding to the cables and antenna holder which are placed behind the antenna during the measurement.

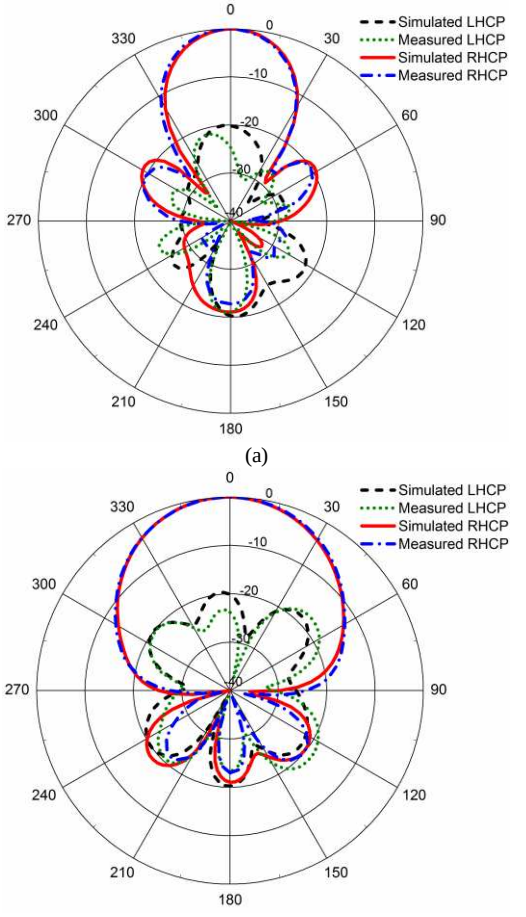

Fig. 19.Simulated and measured radiation patterns of the proposed array: (a) 4GHz XOZ plane, (b) 4GHz YOZ plane, (c) 6GHz XOZ plane, (d) 6GHz YOZ plane.

Fig. 20 shows the measured and simulated gain of the presented antenna array. As shown, the measured gain is around 12-14dBic from 4GHz to 6GHz. The simulated insertion loss of the array feeding network is around 0.5-1.2dB from 4GHz to 6GHz. The difference of the gain between the array and the antenna element increases as frequency goes higher, which mainly attributes to the decreased mutual coupling at higher frequency. Besides, the increase of the ground plane size has some effect on the antenna gain as well. The simulated efficiency of the antenna array, as shown in Fig. 20, is larger than 85% from 4GHz to 6GHz.

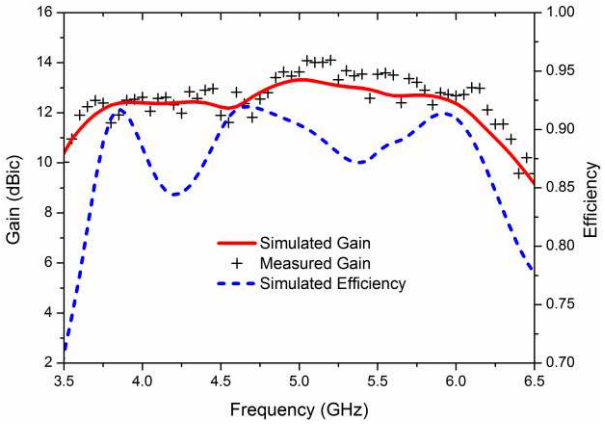

Fig. 20. Gain and simulated efficiency of the antenna array.

V. Conclusion

A wideband CP antenna with wide AR beamwidth within its operational bandwidth is presented in this paper. The proposed S-shaped antenna achieved a CP bandwidth of 42% and over 140° AR beamwidth, leading to a wider CP bandwidth compared with other reported wide AR beamwidth CP antennas. Besides, the AR beamwidths of the presented antenna were larger than the HPBWs in other elevation planes. Due to its simple configuration, the presented antenna can be easily extended to an array antenna with 60% CP bandwidth. Owing to these advantages, the proposed antenna is promising for the applications in GNSS systems and wide-angle CP beam-scanning array antennas.

References

[1] S. Gao, Q. Luo, and F. Zhu, Circularly polarized antennas: John Wiley & Sons, 2013.
[2] H. Iwasaki, "A circularly polarized small-size microstrip antenna with a cross slot," Antennas and Propagation, IEEE Transactions on, vol. 44, pp. 1399-1401, 1996.
[3] Y.-X. Guo, K.-W. Khoo, and L. C. Ong, "Wideband circularly polarized patch antenna using broadband baluns," Antennas and Propagation, IEEE Transactions on, vol. 56, pp. 319-326, 2008.
[4] R. B. Waterhouse, "Stacked patches using high and low dielectric constant material combinations," Antennas and Propagation, IEEE Transactions on, vol. 47, pp. 1767-1771, 1999.
[5] J. Wu, Y. J. Cheng, and Y. Fan, "Millimeter-Wave Wideband High-Efficiency Circularly Polarized Planar Array Antenna," Antennas and Propagation, IEEE Transactions on, vol. 64, pp. 535-542, 2016.
[6] M. Li and K.-M. Luk, "A wideband circularly polarized antenna for microwave and millimeter-wave applications," Antennas and Propagation, IEEE Transactions on, vol. 62, pp. 1872-1879, 2014.
[7] J. J. Wang, "Antennas for global navigation satellite system (GNSS)," Proceedings of the IEEE, vol. 100, pp. 2349-2355, 2012.
[8] X. Bai, S.-W. Qu, S. Yang, J. Hu, and Z.-P. Nie, "Millimeter-Wave Circularly Polarized Tapered-Elliptical Cavity Antenna with Wide Axial-Ratio Beamwidth," Antennas and Propagation, IEEE Transactions on, vol. 64, pp. 811-814, 2016.
[9] X. Qing and Z. N. Chen, "A compact circularly polarized slotted patch antenna for GNSS applications," Antennas and Propagation, IEEE Transactions on, vol. 62, pp. 6506-6509, 2014.
[10] Y. Anjani and A. Alphones, "A Wide-Beam Circularly Polarized Asymmetric-Microstrip Antenna," Antennas and Propagation, IEEE Transactions on, vol. 63, pp. 3764-3768, 2015.
[11] K.-B. Ng, C. H. Chan, and K.-M. Luk, "Low-Cost Vertical Patch Antenna With Wide Axial-Ratio Beamwidth for Handheld Satellite Communications Terminals," Antennas and Propagation, IEEE Transactions on, vol. 63, pp. 1417-1424, 2015.
[12] S. X. Ta, H. Choo, I. Park, and R. W. Ziolkowski, "Multi-band, wide-beam, circularly polarized, crossed, asymmetrically barbed dipole antennas for GPS applications," Antennas and Propagation, IEEE Transactions on, vol. 61, pp. 5771-5775, 2013.
[13] S.-L. Zuo, L. Yang, and Z.-Y. Zhang, "Dual-Band CP Antenna With a Dual-Ring Cavity for Enhanced Beamwidth," Antennas and Wireless Propagation Letters, IEEE, vol. 14, pp. 867-870, 2015.
[14] X. Bao and M. Ammann, "Dual-frequency dual circularly-polarised patch antenna with wide beamwidth," Electronics letters, vol. 44, pp. 1233-1234, 2008.
[15] Y. Luo, Q.-X. Chu, and L. Zhu, "A low-profile wide-beamwidth circularly-polarized antenna via two pairs of parallel dipoles in a square contour," Antennas and Propagation, IEEE Transactions on, vol. 63, pp. 931-936, 2015.
[16] H. Jiang, Z. Xue, W. Li, and W. Ren, "Broad beamwidth stacked patch antenna with wide circularly polarised bandwidth," Electronics Letters, vol. 51, pp. 10-12, 2014.
[17] K. M. Mak and K. M. Luk, "A circularly polarized antenna with wide axial ratio beamwidth," Antennas and Propagation, IEEE Transactions on, vol. 57, pp. 3309-3312, 2009.
[18] S. X. Ta and I. Park, "Crossed dipole loaded with magneto-electric dipole for wideband and wide-beam circularly polarized radiation," Antennas and Wireless Propagation Letters, IEEE, vol. 14, pp. 358-361, 2015.
[19] D. Yu, S.-X. Gong, Y.-T. Wan, Y.-L. Yao, Y.-X. Xu, and F.-W. Wang, "Wideband omnidirectional circularly polarized patch antenna based on vortex slots and shorting vias," Antennas and Propagation, IEEE Transactions on, vol. 62, pp. 3970-3977, 2014.
[20] K.-F. Hung and Y.-C. Lin, "Novel broadband circularly polarized cavity-backed aperture antenna with traveling wave excitation," Antennas and Propagation, IEEE Transactions on, vol. 58, pp. 35-42, 2010.
[21] P. Hall, J. Dahele, and J. James, "Design principles of sequentially fed, wide bandwidth, circularly polarised microstrip antennas," in Microwaves, Antennas and Propagation, IEE Proceedings H, 1989, pp. 381-389.
[22] R. Bawer and J. Wolfe, "A printed circuit balun for use with spiral antennas," IRE Trans. Microw. Theory Tech, vol. 8, pp. 319-325, 1960.
[23] C. A. Balanis, Antenna theory: analysis and design vol. 1: John Wiley & Sons, 2005.
[24] D. Pozar, "Wideband reflectarrays using artificial impedance surfaces," Electronics Letters, vol. 43, p. 1, 2007.
[25] B. A. Munk, Finite antenna arrays and FSS: John Wiley & Sons, 2003.